Carbohydrate Polymers 197 (2018) 478–489

Contents lists available at ScienceDirect

Carbohydrate Polymers

journal homepage: www.elsevier.com/locate/carbpol

Hyaluronic acid decorated tacrolimus-loaded nanoparticles: Efficient approach to maximize dermal targeting and anti-dermatitis efficacy

Fan Zhuo[a], Mohammed A.S. Abourehab[b,c,*], Zahid Hussain[d,**]

[a] Department of dermatology, The First Affiliated Hospital, Xi'an Medical College, Xi'an, 710077, China
[b] Department of Pharmaceutics, Faculty of Pharmacy, Umm Al-Qura University, Makkah, Saudi Arabia
[c] Department of Pharmaceutics, Faculty of Pharmacy, Minia University, Egypt
[d] Department of Pharmaceutics, Faculty of Pharmacy, Universiti Teknologi MARA (UiTM), Puncak Alam Campus, Bandar Puncak Alam 42300, Selangor, Malaysia

ARTICLE INFO

Keywords:
Atopic dermatitis
Tacrolimus
Hyaluronic acid
Nanoparticles
Efficient dermal targeting
Improved anti-dermatitis efficacy

ABSTRACT

Nano-delivery systems have gained remarkable recognition for targeted delivery of therapeutic payload, reduced off-target effects, and improved biopharmaceutical profiles of drugs. Therefore, we aimed to fabricate polymeric nanoparticles (NPs) to deliver tacrolimus (TCS) to deeper layers of the skin in order to alleviate its systemic toxicity and improved therapeutic efficacy against atopic dermatitis (AD). To further optimize the targeting efficiency, TCS-loaded NPs were coated with hyaluronic acid (HA). Following the various physicochemical optimizations, the prepared HA-TCS-CS-NPs were tested for *in vitro* drug release kinetics, drug permeation across the stratum corneum, percentage of drug retained in the epidermis and dermis, and anti-AD efficacy. Results revealed that HA-TCS-CS-NPs exhibit sustained release profile, promising drug permeation ability, improved skin retention, and pronounced anti-AD efficacy. Conclusively, we anticipated that HA-based modification of TCS-CS-NPs could be a promising therapeutic approach for rationalized management of AD, particularly in children as well as in adults having steroid phobia.

1. Introduction

Atopic dermatitis (AD) is a chronic inflammatory skin disease characterised by severe itching, rashes, and inflammatory reactions. The prevalence of AD is about 20 percent in Malaysia and Singapore with 90 percent of suffers developing the condition before age of 5 years (Tay, Kong, Khoo, Goh, & Giam, 2002). To date, there is no absolute therapy for the treatment of AD due to its complex pathogenic interplay between patient's susceptible genes, skin barrier abnormalities, and immune deregulation (Bieber, 2008). Various pharmacological and non-pharmacological approaches including identification and avoidance of causative allergens, skin hydration (baths, using moisturizer), wet-wrap dressings, topical anti-inflammatory and immunosuppressant therapies (topical corticosteroids (TCs) and topical calcineurin inhibitors (TCIs)), antipruritic medications and anti-bacterial measures (bleach baths, antiseptics, and disinfectants) have been used, alone or in combination, for the management for mild-to-severe AD (Hussain et al., 2016). Among various pharmacological interventions, TCs are the mainstay choice for the treatment of AD; however due to its numerous local and systemic adverse effects, these are generally recommended for a shorter period (not more than 3 weeks) and are less commonly prescribed in children (Zöller et al., 2008). Alternatively, TCIs (*e.g.*, tacrolimus and pimecrolimus) are being used as promising therapeutic agents because these agents can be used for longer time and be equally effective and safe in both the children and young adults (Yin, Xu, & Luo, 2011).

Nanomedicines have gained remarkable recognition from researchers around the globe due to their promising potential advantages including target-specific delivery of pharmacological moieties, ultra-small size, surface charge, high entrapment efficiency, non-target accumulation of drug contents, and improved biopharmaceutical and therapeutic efficacy (Hussain, Katas, Mohd Amin, Kumulosasi, Buang, et al., 2013; Hussain, Katas, Mohd Amin, Kumulosasi, & Sahudin, 2013; Shao et al., 2016). These advanced delivery systems include liposomes, nanoemulgel, ethosomes, solid lipid nanoparticles, micelles, and polymeric nanoparticles (NPs) (Shao et al., 2016). Among various nanodelivery systems, polymeric NPs have gained greater popularity from scientists around the globe (Hussain, Katas, Mohd Amin, & Kumolosasi, 2014). The success of the polymeric NPs is due to their numerous characteristic features including ultra-small particle size, surface

* Corresponding author at: Department of Pharmaceutics, Faculty of Pharmacy, Umm Al-Qura University, Makkah, Saudi Arabia.
** Corresponding author at: Department of Pharmaceutics, Faculty of Pharmacy, Universiti Teknologi MARA (UiTM), Puncak Alam Campus, Bandar Puncak Alam 42300, Selangor, Malaysia.
E-mail addresses: maabourehab@uqu.edu.sa (M.A.S. Abourehab), zahid3224@puncakalam.uitm.edu.my (Z. Hussain).

https://doi.org/10.1016/j.carbpol.2018.06.023
Received 12 December 2017; Received in revised form 13 April 2018; Accepted 5 June 2018
Available online 06 June 2018
0144-8617/

charge, biocompatibility, and biodegradability (Shao et al., 2016). Polymeric NPs are also suitable for topical delivery of a wide range of drugs because of their exceptional pharmaceutical properties including sustained release, high entrapment efficiency, prevention of enzymatic degradation, and efficient triggered release of the encapsulated payload in response to physiological stimuli, variation in pH and presence or absence of biological catalysts (enzymes) as well as their ability of target-specific delivery of drugs to minimise off-target effects (Wu, Price, & Guy, 2009). Due to the aforementioned biopharmaceutical and therapeutic advantages, we aimed to delivery tacrolimus to deeper layers of the skin for dermal targeting and rational treatment of AD.

To further optimize the targeting efficiency and therapeutic efficacy of the tacrolimus (TCS), the prepared NPs were coated with hyaluronic acid (HA). Because of a wide range of pharmacological activities, HA has been widely used as wound healing and tissue regenerating agent (Hussain, Thu, Katas, & Bukhari, 2017), anticancer (Safdar et al., 2017), anti-inflammatory, moisturizing, and cosmeceutical agent. Moreover, according to a study by Witting et al. (2015), HA remarkably enhanced the penetration of encapsulated drugs into the deeper layers of the skin. Having all these features of HA, we anticipate that HA based coating of TCS-loaded NPs will improve penetration ability of TCS across the SC, achieve superior dermal targeting, and improved anti-AD efficacy.

The present study was therefore aimed to fabricate HA-coated TCS-CS-NPs with optimal physicochemical characteristics (*i.e.*, particle size, polydispersity index (PDI), zeta potential, encapsulation efficiency (EE), loading capacity, morphology, FTIR, XRD, and TGA). The fabricated HA-TCS-CS-NPs were further assessed for *in-vitro* release kinetics, drug permeation efficiency across the full thickness NC/Nga mice, and drug retention into the various skin layers. Taken together, the therapeutic efficacy of the prepared HA-TCS-CS-NPs was evaluated by assessing the transepidermal water loss (TEWL), erythema intensity, AD severity scores, and histological examination.

2. Materials and methods

2.1. Materials

Eight-week-old NC/Nga mice were purchased from RIKEN BioResource Center, Japan. Isoflurane (inhalation anesthetic) was obtained from Piramal Healthcare Limited, Kuala Lumpur, Malaysia. Low molecular weight chitosan (MW, 70 kDa; deacetylation degree, 85%), polyvinyl alcohol, tacrolimus, phosphate buffered saline, and hyaluronic acid (100 kDa) were sourced from Sigma-Aldrich Chemicals Co. Ltd. (Kuala Lumpur, Malaysia). All other chemicals were of analytical grade and were sourced from Fundamental of Pharmaceutics Laboratories, Universiti Teknologi MARA, Malaysia.

2.2. Preparation of unloaded CS-NPs: high pressure homogenization method

The unloaded CS-NPs were prepared using high pressure homogenization– evaporation method (Pandey et al., 2018). Briefly, 0.5% (w/v) CS solution was prepared by dissolving 2.0 g of CS in 400 mL of acidified water (1% v/v acetic acid into 100 mL of distilled water) and was homogenized using high speed stirrer homogenizer (D-Series Benchtop Homogenizer, USA) at 10,000 rpm for 30 min. Afterward, 2.0 g of polyvinyl alcohol (PVA) was dissolved in 24 mL of dichloromethane and the final solution was added to CS solution and homogenized for 30 min. Finally, the mixture was subjected to high pressure homogenization (Next Generation Homogenizer, Nano DeBee, USA) for 5 cycles at 20,000 PSI for the formation of unloaded CS-NPs. The CS-NPs dispersion was also subjected to sonication (10 min) during the process of high pressure homogenization.

2.2.1. Optimization of formulation and process parameters

The unloaded CS-NPs were further optimized for formulation (*e.g.*, PVA and CS concentrations) and process parameters (*e.g.*, homogenization cycles and pressure). In due course, only one variable was changed in each set of experiments. To analyse the effect of different amounts of PVA (0.5, 1.0, 1.5 and 2.0 g), other formulation conditions such as amount of CS (2.0 g), dichloromethane (6 mL), homogenization cycles (five), homogenization pressure (20,000 PSI), homogenization time (30 min), and sonication time (10 min) were kept constant. Similarly, to analyse the effect of different concentrations of CS (1.0, 2.5, 5.0, 7.5, 10.0 mg/mL), amount of PVA (2.0 g), dichloromethane (6 mL), homogenization cycles (five), homogenization pressure (20,000 PSI), homogenization time (30 min), and sonication time (10 min) were kept constant. Similarly, the effect of different formulation parameters such as number of homogenization cycles (5, 6, 7, 8, 9, and 10) and homogenization pressure (10,000, 15,000, 20,000, 25,000, and 30,000 PSI) has also been investigated. Finally, the prepared CS-NPs were physicochemically characterized (particle size, zeta potential, polydispersity index, entrapment efficiency, and loading capacity) after a ten-fold dilution of each sample.

2.3. Optimization of TCS-CS-NPs and effect of HA coating

Prior to performing optimization of TCS-CS-NPs, TCS was dissolved in ethanol using the magnetic stirrer for 10 min. TCS-CS-NPs were optimized at different TCS concentrations (0.01, 0.02, 0.03, 0.04, and 0.05% w/v) at constant pre-determined formulation and process parameters including CS concentration (0.5% w/v), amount of PVA (1.0 g), homogenization cycles (five), homogenization pressure (20,000 PSI) and sonication time (10 min).

To further expand the physicochemical characteristics, pharmaceutical viability, and therapeutic efficacy, the TCS-CS-NPs were coated with different concentrations of HA (0.1, 0.2, 0.3, 0.4, and 0.5% w/v). In order to optimize the coating of HA, TCS-CS-NPs dispersion was kept on magnetic stirring overnight for solvent evaporation prior to incubate with different concentrations of HA for a period of 3 h under constant magnetic stirring. Finally, the prepared TCS-CS-NPs and HA-TCS-CS-NPs were harvested by ultracentrifugation (25,000 rpm) using an Optima L-100 XP Ultracentrifuge (Beckman-Coulter, USA) for 30 min at 25 °C. The resulting NPs pellets were lyophilized for further analysis. Prior to undergo lyophilisation process, 2.0 g of mannitol was added to each sample as a cryoprotectant.

2.4. Physicochemical characterization

The prepared TCS-CS-NPs and HA-TCS-CS-NPs were tested for various physicochemical characteristics (particle size, zeta potential, PDI, entrapment efficiency, and loading capacity).

2.4.1. Particle size (nm), PDI, and zeta potential (mV)

The mean particle size, PDI, and zeta potential of TCS-CS-NPs and HA-TCS-CS-NPs were analysed using dynamic laser light scattering (DLS) method using Malvern Nano-ZS Zetasizer (Malvern Instruments, Malvern, UK). All measurements were performed in triplicates at a scattering angle of 90° at room temperature. The results were reported as mean ± standard deviation (S.D).

2.4.2. Measurement of entrapment efficiency (%EE) and loading capacity (%LC)

To measure %EE and %LC, the TCS-CS-NPs and HA-TCS-CS-NPs were harvested by ultracentrifugation (25,000 rpm) using an Optima L-100 XP Ultracentrifuge (Beckman-Coulter, USA) for 30 min at 25 °C. The concentrations of TCS in the supernatants were analysed using Shimadzu UV–vis Spectrophotometer (model UV-1800) at 294 nm. The %EE and %LC were calculated using the following equations:

$$\text{Entrapment efficiency (EE) (\%)} = (W_t - W_f)/W_t \times 100$$

$$\text{Loading capacity (LC) (\%)} = (W_t - W_f)/W_n \times 100$$

Where W_t is the total initial amount of TCS and W_f is the amount of free drug in the supernatant after ultracentrifugation. W_n is the average weight of lyophilized TCS-CS-NPs or HA-TCS-CS-NPs All the measurements were performed in triplicates and were reported as mean ± SD (n = 3).

2.5. Morphological examination

The morphological examination of synthesized HA-TCS-CS-NPs was executed using scanning electron microscopy (SEM) (Zeiss Sigma 300 VP-FESEM). To evaluate the morphological features, the lyophilized HA-TCS-CS-NPs sample was efficiently dispersed in ethanol by sonication (5 min). The NPs dispersion was then coated with platinum (~20 nm thick) using an Ion Sputter (JFC-1100, JEOL Ltd., Tokyo, Japan) for 5 min at 20 mA. The microscopic observation was performed at an accelerating voltage of 5 kV and a working distance of 10 mm. The morphological analysis of HA-TCS-CS-NPs was executed at a magnification of 5000× and 10,000× (Amidi et al., 2006).

2.6. Fourier transform infra-red spectroscopy (FT-IR)

For FT-IR analysis, approximately 2–3 mg of lyophilized HA-TCS-CS-NPs powder was ground with 78 mg of potassium bromide (KBr) and compressed into a transparent pellet using hydraulic press. Notably, the lyophilized samples of HA-TCS-CS-NPs were kept in oven overnight prior to grinding with KBr. Similar method was used to produce transparent pellets of pure CS, TCS, and HA samples, respectively. Then the resulting pellets were scanned for IR analysis using FT-IR spectrophotometer (Spectrum 100; Perkin Elmer, USA) at a spectral region of 4000–400 cm^{-1}. A resolution of 4 cm^{-1} and 16 scans were obtained for each spectrum.

2.7. Thermo-gravimetric analysis (TGA)

To determine the thermal stability of the prepared HA-TCS-CS-NPs, TGA analysis (Perkin Elmer Model, USA) was performed. The samples were analysed in the temperature ranges from 50 to 600 °C with heating rate of 10 °C/min under nitrogen atmosphere at a flow rate of 50 cm^3/min (Benoit et al., 2012). The weight of the test samples containing pan was recorded constantly as a function of temperature.

2.8. X-ray diffraction (XRD) analysis

To determine the crystallinity or amorphous nature of the synthesized HA-TCS-CS-NPs, XRD analysis was performed using X-ray diffractometer (RIGAKU ULTIMA IV, TYPE II, HE-2001Q) equipped with Cu Kα radiation at a voltage of 40 kV and a generator current of 100 mA. The diffractograms of all samples were recorded in the range of 2θ = 1–100° at a scanning rate of 2°/min (Katas & Alpar, 2006; Parida, Rout, & Bindhani, 2013).

2.9. In vitro release kinetics

In vitro release kinetics of TCS from TCS-CS-NPs and HA-TCS-CS-NPs were determined using a previously developed method (Hussain, Katas, Mohd Amin, Kumulosasi, Buang, et al., 2013) with slight modifications. Briefly, 50 mg of lyophilized TCS-CS-NPs were re-dispersed in 5 mL of freshly prepared PBS solution having 0.01% Tween 20 and placed into the dialysis tube (MWCO: 12000). The dialysis tube (containing NPs dispersion) was then submerged in 200 mL of dissolution media (PBS + 0.01% Tween 20) at pH 7.4. The beaker was continuously shaken with 100 stocks/min at 37 ± 0.5 °C using Certomat S II Orbital Benchtop Shaker. At pre-determined time intervals, 5 mL of the dissolution media was withdrawn and replaced with 5 mL of fresh dissolution media to maintain sink conditions constant. The concentration of TCS released into the dissolution medium was measured using UV–vis spectrophotometer at 294 nm. The cumulative release of TCS was calculated using the standard calibration curve. A similar method was used to determine the release profile of TCS from HA-TCS-CS-NPs.

2.10. Ex vivo drug permeation

Despite of analysing the release profile of TCS in *in vitro* experimental conditions, the drug permeation efficiency of TCS-CS-NPs and HA-TCS-CS-NPs across the full-thickness NC/Nga mouse skin was also evaluated. For that, NC/Nga mice were sacrificed and hairs on the dorsal side were removed using hair clipper (Aesculap, Germany) taking extreme precaution to avoid skin abrasions. Skin from dorsal body region was then excised and subcutaneous tissues were surgically removed. The excised skin was then washed with PBS and carefully wiped from the dermal side using cotton swabs dipped in isopropyl alcohol to remove adhering fats and then wrapped in an aluminium foil and stored at −20 °C for further analysis.

The *ex vivo* drug permeation experiments were performed using jacketed Franz diffusion cells (PermeGear, Inc., USA) consisting of 6 cells having a diffusional surface area of 0.654 cm^2 and a receptor cell volume of 5 mL operated at continuous stirring mode (600 rpm) at 37 °C (Hussain, Katas, Mohd Amin, Kumulosasi, Buang, et al., 2013). The receptor compartments were filled with a mixture of PBS + 0.01% Tween 20 at pH 7.4. Prior to the experiment, the frozen dermatomed mouse skin was thawed at room temperature, rehydrated with PBS + 0.01% Tween 20 (pH 7.4) at 37 °C for 1 h and immediately mounted on to the diffusion cell with the SC facing the donor compartment. Then, the donor compartment was equilibrated with the receiver compartment solution for 1 h to further facilitate skin hydration. For all permeation experiments, the cumulative permeated flux of TCS at different time intervals was estimated using UV–vis spectrophotometer.

The permeation flux (μg/cm^2/h) of TCS was calculated from the slope of the plot of cumulative amount of permeated drugs from the dermatomed mouse skin *versus* time by using linear regression analysis. The permeability coefficient (Kp) of TCS across the dermatomed mouse skin was approximated using the following equation:

$$\text{Permeability coefficient (Kp)} = J/C$$

Where J is the flux and C is the concentration of TCS in the donor compartment.

2.11. Estimation of TCS retained in the epidermis and dermis

Following the permeation experiment, the dermatomed mouse skin mounted on the Franz diffusion cells was carefully removed. To determine the percentage of TCS retained into various skin layers (epidermis and dermis), the cleaned dermatomed mouse skin was subjected to heat separation technique (Padula, Sartori, Marra, & Santi, 2005) to separate the epidermis from the dermis. Subsequently, the epidermis and dermis were weighed and extracted with 10 mL of methanol by mechanically shaking in a water bath (BW-20 G, Lab. Companion, USA) at 37 ± 1 °C overnight. To further improve the extraction efficiencies, tissue cell lysis reagent (T-PER) was also introduced at a ratio of 1:20 of tissue to T-PER and sonicated (EUROSTAR digital, IKA®, Malaysia) for 30 min. Afterward, all samples were harvested by ultracentrifugation (12,000 rpm) at 10 °C for 20 min. The quantification of TCS in the epidermis and dermis was performed using UV–vis spectrophotometer by normalizing the amount of drug recovered in the epidermis and dermis by the weight of tissue and expressed as micrograms of drug per gram of tissue.

2.12. Pre-clinical evaluation

2.12.1. Experimental protocol

The preclinical evaluation and therapeutic efficacy of HA-TCS-CS-NPs based topical formulation was assessed using NC/Nga mice (8-weeks-old). The animals were housed in an "Individual Ventilated Cage" (IVC) assembly with inlet air filters in an air-conditioned room with 12-h light/12-h dark cycle at a temperature of 23 ± 1 °C and a humidity of 60 ± 5%. Mice were provided with a laboratory diet and water *ad libitum*. The experimental protocol for animal handling was in accordance with the National Institute of Health (NIH) guidelines and approved by the Animal Ethics Committee of Universiti Teknologi MARA.

AD was induced by the application of 100 µL of 0.15% solution of 2,4-dinitroflourobenzene (DNFB) in acetone/olive oil (3:1) onto the shaved dorsal skin of the anesthetised mice once on day 1 and again on day 5. On days 9, 11, and 13, mice were sensitised again by application of 100 µL of 0.2% DNFB on the dorsal skin as described previously (Hussain, Katas, Mohd Amin, Kumulosasi, 2014). The NC/Nga mice were randomly divided into 6 groups (n = 8). The normal mice were considered as the baseline group to compare the physiological skin conditions. The second group was considered the AD group that received repeated DNFB applications without any treatment. Third group was positive control group which included AD-induced mice treated with commercial 0.03% tacrolimus ointment. The fourth group was containing AD-induced mice treated with TCS solution. The fifth (TCS-CS-NPs) and sixth (HA-TCS-CS-NPs) mice groups were AD-induced mice that were treated with TCS-CS-NPs and HA-TCS-CS-NPs nanoformulations.

2.12.2. Therapeutic efficacy

The therapeutic efficacy of test nanoformulations was assessed by evaluating the TEWL, erythema intensity, and dermatitis index.

2.12.2.1. TEWL and erythema intensity. TEWL ($g/m^2/h$) and erythema intensity of experimental animals were determined using Tewameter® TM 300 (Courage and Khazaka electronic GmbH, Germany) and Mexameter® MX 18 (Courage and Khazaka electronic GmbH, Germany), respectively. The mice in the normal, control, and treatment groups were isolated in an air conditioned room (20 ± 3 °C) with a relative humidity of 50–60% for 30 min before each testing session. Then, the TEWL (g/m2/h) and erythema intensity were measured within 0.5–3 h after application of tested formulation.

2.12.2.2. Dermatitis index. Severity of AD was assessed by 2 medical professionals blind to treatment conditions of the mice according to the criteria described previously (Park et al., 2007). The severity of AD was evaluated as a dermatitis index/score established according to the following criteria: (1) erythema/haemorrhage, (2) dryness/scaling, (3) oedema/swelling, and (4) erosion/excoriation, each of which were scored as 0 (none), 1 (mild), 2 (moderate), or 3 (severe). The sum of the individual scores was then taken as the dermatitis index. Moreover, to harmonize the data and to clarify equivocal responses, the severity of AD was further evaluated by examining the dorsal skin of anesthetized NC/Nga mice under an advanced digital light microscope (Dino-Lite®).

2.13. Histological examination

Dorsal skin specimens (5 mm) obtained after euthanization of NC/Nga mice were punched by skin biopsy needle and fixed in 10% buffered formalin. Skin specimens were then processed by a series of solvents, embedded in paraffin wax, and serially sectioned (5 mm) using a microtome. Sections were affixed to glass sample slides by the fishing method. Slides were then rehydrated and dehydrated by bathing them in various concentrations of alcohol (95%, 80%, 70%, and 50% v/v). Then, slides were stained with hematoxylin-eosin (H & E) stain to examine histopathology of the skin. Finally, the stained skin specimens were examined for various pathological changes in the skin infrastructure under a light microscope with image analysis software (VideoTesT-Master Morphology: Video TesT, St Petersburg, Russia). The histopathologic severity of AD was assessed by 2 veterinary pathologists according to the following criteria: (1) fragmentation of keratinised epithelium, (2) acanthosis, (3) numbers of inflammatory cells infiltrated in the dermis, and (4) hyperkeratosis. Each of the criteria was scored as 0 (none), 1 (mild), 2 (moderate), or 3 (severe). The sum of the individual scores was then taken as histopathologic scores (HPS) of group tested.

2.14. Statistical analysis

All data were presented as mean ± standard deviation (S.D). Data were statistically analysed using paired *t*-test and one-way analysis of variance (ANOVA) followed by Tukey's *post hoc* analysis using SPSS Inc. statistical software. A "*p*" value of < 0.05 was considered statistically significant.

3. Results and discussion

3.1. Optimization of formulation and process parameters

3.1.1. Effect of PVA concentrations

The effects of different concentrations (0.5, 1.0, 1.5 and 2.0 g) of PVA on the physicochemical characteristics of TCS-CS-NPs and HA-TCS-CS-NPs were evaluated and results are presented in Table 1. Results depicted that the average particle size of the unloaded CS-NPs was significantly ($p < 0.05$, paired *t*-test) increased from 95 ± 11 to 146 ± 13 nm, when the amount of PVA was increased from 0.5 to 2.0 g. On the other hand, zeta potential was varied from +63.7 ± 6.7 to +67.5 ± 9.3 mV at different concentrations of PVA which indicates stability of the formulation because the NPs dispersion with zeta potentials greater than ± 30 mV is considered to remain stable in the medium (Bhattacharjee, 2016). A narrow size distribution index (low value of PDI) also demonstrates stability of NPs dispersion (0.221 ± 0.075 to 0.321 ± 0.066). Though, 0.5 g of PVA produced the smallest particle size; however, we have chosen 1.0 g of PVA as the optimal amount of cross-linker due to the fact that sufficient amount of cross-linker (PVA) is needed to keep the NPs dispersion stable (Mainardes & Evangelista, 2005; Sharma, Madan, & Lin, 2016).

3.1.2. Effect of CS concentration

Effects of another formulation variable (CS concentration) on the physicochemical characteristics of the unloaded CS-NPs were also evaluated (Table 1). Results showed that the average particle size of the unloaded CS-NPs was significantly ($p < 0.05$, paired *t*-test) increased from 86 ± 12 to 276 ± 25 nm, when CS concentration was increased from 1.0 to 10.0 mg/mL (Table 1). Similarly, a consistent increase in the zeta potential from +50.6 ± 8.5 to +67.8 ± 7.5 mV was observed, when the CS concentration was increased from 1.0 to 10.0 mg/mL (Table 1). The increase in zeta potential is expected to be due to the increased number of amino groups on the contour of CS-NPs (Hussain, Katas, Mohd Amin, Kumulosasi, Buang, et al., 2013; Kalam, 2016). On the other hand, the smaller values of PDI indicate a narrow size distribution which may assist in enhancing the stability of the NPs dispersion in the medium (Kalam, 2016). We selected 5.0 mg/mL of CS concentration as the optimal concentration due to producing smallest particle size (117 ± 19 nm), highest zeta potential (+63.8 ± 6.4 mV), and narrow size distribution index (0.262 ± 0.049) for further analysis.

3.1.3. Effect of process parameters

Despite of analysing the effects of formulation parameters (PVA and CS concentrations), various process parameters (homogenization cycles

Table 1
Optimization of physicochemical characteristics of unloaded CS-NPs at various formulation and process parameters (data represented as mean ± SD, n = 3).

Formulation and process parameters		Particle size Mean ± S.D (nm)	PDI Mean ± S.D	Zeta potential Mean ± SD (mV)
Amount of PVA (g)	0.5	96 ± 11	0.321 ± 0.066	+63.7 ± 6.7
	1.0	112 ± 12	0.221 ± 0.075	+66.6 ± 4.9
	1.5	132 ± 15	0.248 ± 0.096	+67.5 ± 9.3
	2.0	146 ± 13	0.256 ± 0.011	+63.2 ± 11.7
CS concentration (mg/mL)	1.0	86 ± 12	0.180 ± 0.099	+50.6 ± 8.5
	2.5	97 ± 11	0.239 ± 0.089	+57.2 ± 10.3
	5.0	117 ± 19	0.262 ± 0.049	+63.8 ± 6.4
	7.5	198 ± 21	0.309 ± 0.086	+64.1 ± 4.3
	10.0	276 ± 25	0.344 ± 0.072	+67.8 ± 7.5
Homogenization cycles	5	149 ± 11	0.261 ± 0.076	+62.7 ± 4.48
	6	131 ± 17	0.297 ± 0.049	+59.2 ± 6.43
	7	116 ± 14	0.258 ± 0.028	+57.2 ± 5.51
	8	115 ± 16	0.341 ± 0.062	+57.7 ± 3.86
	9	114 ± 11	0.232 ± 0.016	+55.9 ± 3.58
	10	112 ± 13	0.294 ± 0.072	+55.3 ± 3.72
Homogenization pressure (PSI)	10,000	179 ± 13	0.33 ± 0.099	+61.9 ± 6.72
	15,000	152 ± 18	0.28 ± 0.099	+64.6 ± 8.88
	20,000	111 ± 14	0.274 ± 0.038	+62.7 ± 6.99
	25,000	141 ± 11	0.291 ± 0.039	+54.9 ± 8.7
	30,000	198 ± 19	0.45 ± 0.078	+51.5 ± 12.4

Table 2
Optimization of physicochemical characteristics of TCS-CS-NPs and HA-TCS-CS-NPs at different TCS and HA concentrations.

Formulation variables		Particle size (nm) (mean ± S.D)	Zeta potential (mV) (mean ± S.D)	PDI (mean ± S.D)	EE (%) (mean ± S.D)	LC (%) (mean ± S.D)
TCS concentrations (% w/v)	0.01%	156 ± 11	+64 ± 6.62	0.23 ± 0.02	66.51 ± 6.23	16.22 ± 2.24
	0.02%	171 ± 17	+63 ± 4.24	0.31 ± 0.06	73.82 ± 7.15	26.23 ± 4.11
	0.03%	189 ± 23	+61 ± 8.13	0.35 ± 0.11	84.11 ± 4.93	29.12 ± 3.95
	0.04%	253 ± 26	+54 ± 4.31	0.43 ± 0.12	84.32 ± 9.26	31.43 ± 6.11
	0.05%	275 ± 18	+53 ± 8.52	0.51 ± 0.17	86.36 ± 7.16	32.21 ± 7.19
HA concentrations (% w/v)	0.1%	216 ± 16	+51 ± 4.67	0.32 ± 0.04	41.22 ± 4.13	29.23 ± 1.19
	0.2%	223 ± 12	+49 ± 3.94	0.35 ± 0.11	53.39 ± 4.87	29.34 ± 2.13
	0.3%	242 ± 21	+41 ± 5.83	0.26 ± 0.09	55.92 ± 6.91	31.23 ± 3.11
	0.4%	276 ± 31	+37 ± 7.11	0.48 ± 0.08	56.45 ± 4.21	31.43 ± 2.18
	0.5%	389 ± 26	+34 ± 5.23	0.44 ± 0.15	57.14 ± 6.91	33.62 ± 4.71

and pressure) have also been evaluated (Table 1). Results depicted that the mean particle size was gradually decreased from 149 ± 11 to 112 ± 13 nm, when homogenization cycles were increased from 5 to 10, respectively. This might be due to the fact that as the number of homogenization cycles increases, CS-NPs undergo physicochemical transformation that might result into the decreased particle sizes (Peng et al., 2015). Based on the results, we selected seven homogenization cycles as the optimal process variable because further increase in the number of homogenization cycles do not cause significant variations in the particle size and zeta potential.

Similarly, the effect of homogenization pressure has also been evaluated (Table 1). Results showed a consistent decrease in the mean particle size from 179 ± 13 to 111 ± 14 nm, when the homogenization pressure was increased from 10,000 to 20,000 PSI; however above 20,000 PSI, a significant increase in the mean particle size was observed. On the other hand, no significant variation in the zeta potential was observed, when the pressure increases from 10,000 to 20,000 PSI; however, a consistent decrease in the zeta potential was observed when homogenization pressure was further increased from 25,000 to 30,000 PSI. This could be due to inadequate emulsification when homogenization pressure was increased above 20,000 PSI which resulted in agglomeration of the NPs and ultimately enhanced particle sizes (Zu et al., 2014). The optimized homogenization pressure selected for further analysis was 20,000 PSI.

3.2. Optimization of TCS-CS-NPs and HA-TCS-CS-NPs

After optimizing the formulation and process parameters, TCS-CS-NPs and HA-TCS-CS-NPs were further optimized at various TCS and HA concentrations (Table 2). Results depicted that the mean particle size of TCS-CS-NPs was increased from 156 ± 11 to 275 ± 18 nm, when the concentration of TCS was increased from 0.01 to 0.05% w/v, respectively. These results are in agreement with a previous study by Sharma et al. (2016) who reported that an increase in the concentration of drug (s) in the nanoemulsion results in an increase in the mean particle size of the NPs. Moreover, the zeta potential was consistently decreased from +64 ± 6.62 to +53 ± 8.52 mV, when the TCS concentration was gradually increased (Sharma et al., 2016).

Our results also revealed that %EE of TCS-CS-NPs was significantly ($p < 0.05$, one way ANOVA) increased from 66.51 ± 6.23 to 84.11 ± 4.93%, when the concentration of TCS was increased from 0.01 to 0.03% w/v; however, further increase in the concentration of TCS does not increase %EE (Table 2). These results are expected to be due to the fact that an optimum concentration of a drug can be incorporated into a specific amount of polymer (CS) and further increase in the drug concentration could only lead to enhance viscosity of the solution and thus produce larger particles (Sharma et al., 2016).

Based on our objectives of producing the TCS-CS-NPs with optimum physicochemical characteristics *i.e.*, smallest particle size, higher zeta potential, %EE, and % yield (%LC), we selected 0.03% w/v TCS concentration as the final concentration. The optimized TCS-CS-NPs were then coated with different concentrations of HA and the results are

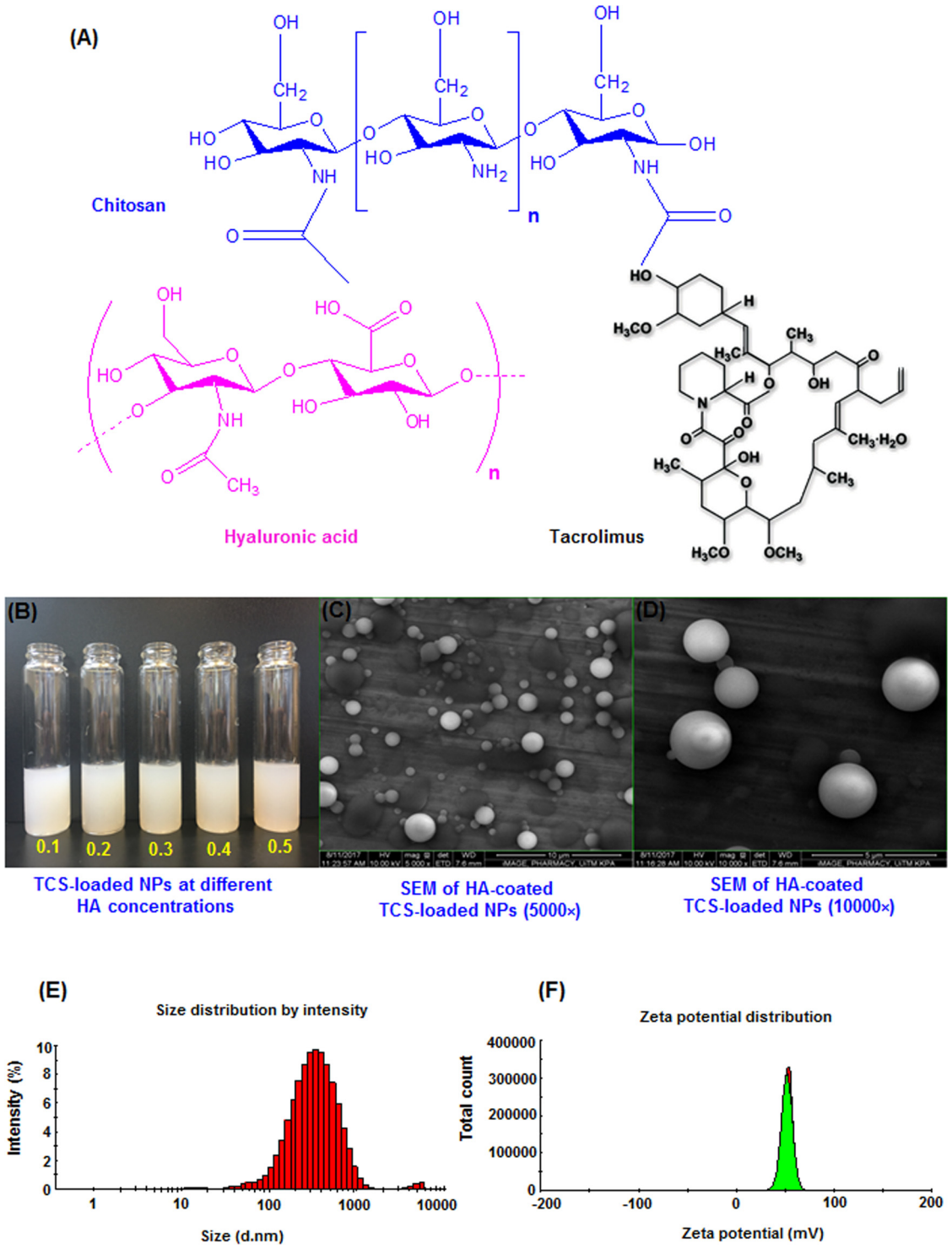

Fig. 1. (A) chemical structure of CS, TCS, and HA, (B) dispersions of HA-TCS-CS-NPs at different HA concentrations (0.1, 0.2, 0.3, 0.4, and 0.5 mg/mL), (C) SEM micrographs of optimized HA-TCS-CS-NPs prepared with 0.03% w/v TCS and 0.2% w/v concentration of HA at 5000×, (D) 10,000× resolutions, (E) particle size distribution by intensity histogram, and (F) zeta potential distribution histogram.

presented in Table 2. Results showed that as the concentration of HA increases from 0.1 to 0.5% w/v, a consistent increase in the average particle size ($p < 0.05$, paired *t*-test) of HA-TCS-CS-NPs from 216 ± 16 to 389 ± 26 nm was observed. On the other hand, the zeta potential was consistently decreased from +51 ± 4.67 to +34 ± 5.23 mV, when the concentration of HA was increased. This might be due to the adsorption of negatively charged HA on to the surface of positively charged TCS-CS-NPs due to ionic interactions between the oppositely charged molecules (Wang, Hou, Su, Zhao, & Shi, 2017). As a result of the decline in the surface charge of NPs, the mean particle size of HA-TCS-CS-NPs increases by increasing the concentration of HA. Interestingly, the zeta potential values of all HA-TCS-CS-NPs formulation prepared at different concentrations of HA were higher than ± 30 mV which prevent particle agglomeration and keep nanoformulation stable (Bhattacharjee, 2016; Maiolino et al., 2015). Results also showed that %EE was gradually increased from 41.22 ± 4.13 to 57.14 ± 6.91%,

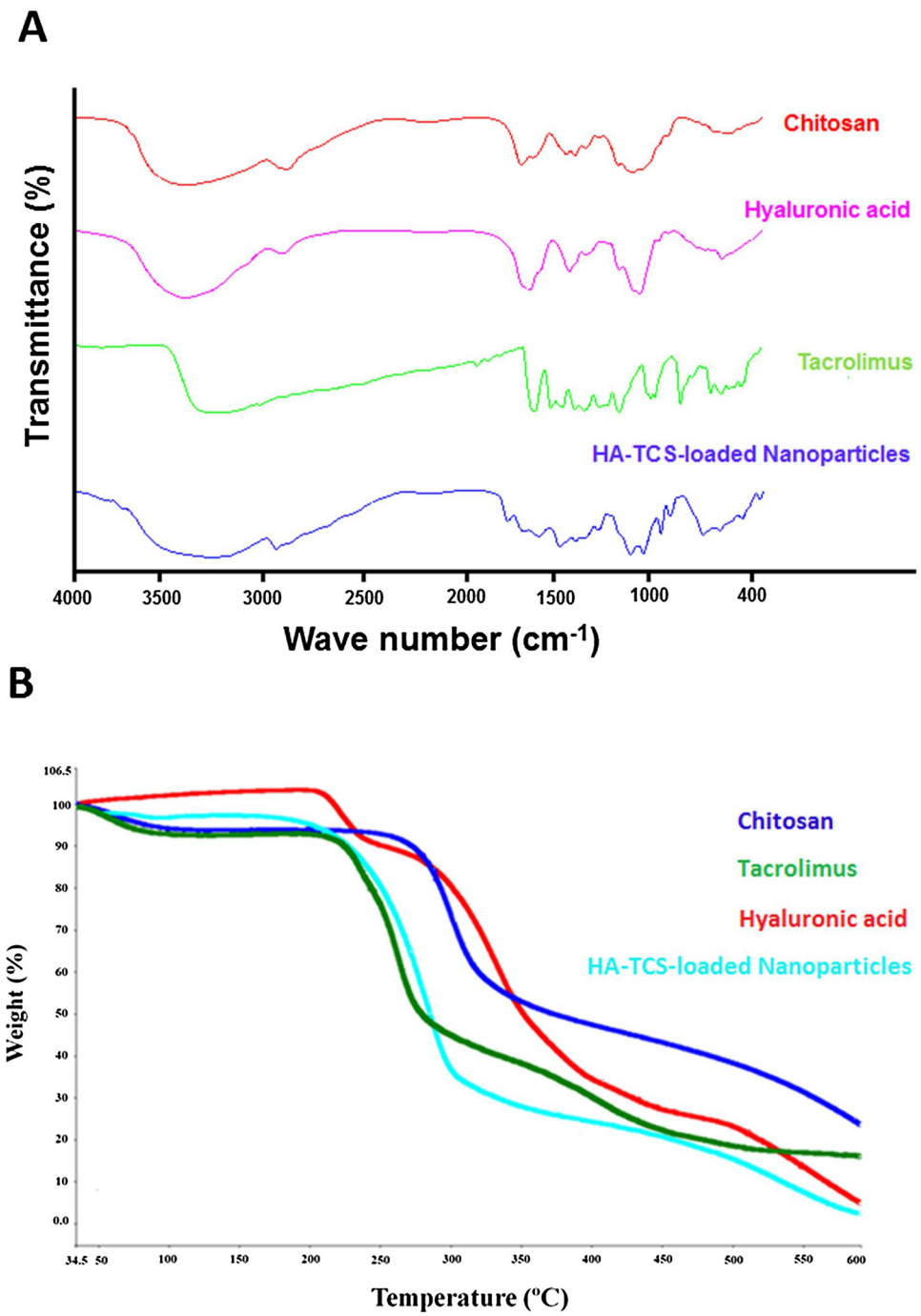

Fig. 2. (A) FT-IR spectra of chitosan, hyaluronic acid, tacrolimus, and HA-TCS-CS-NPs and (B) TGA spectra of chitosan, tacrolimus, hyaluronic acid, and HA-TCS-CS-NPs.

when the concentration of HA was increased. After the data analysis, we selected 0.2% w/v concentration of HA as the final concentration for decorating the TCS-CS-NPs due to producing optimal particle size (223 ± 12 nm), zeta potential (+49 ± 3.94 mV), %EE (53.39 ± 4.87%), and %LC (29.34 ± 2.13%) of HA-TCS-CS-NPs.

3.3. Morphological examination

To examine the surface morphology of the optimized HA-TCS-CS-NPs prepared with 0.03% w/v TCS and 0.2% w/v concentration of HA, SEM analysis was executed. The resulting micrographs revealed that HA-TCS-CS-NPs exhibited smooth surfaces with uniform solid dense spherical shape (Fig. 1). The dispersed light grey spheres that are surrounded by a darker rim likely corresponding the coating with HA [29]. The HA coating improved the appearance and resulted in a slight increase in the mean particle size of HA-TCS-CS-NPs.

3.4. FT-IR analysis

FT-IR spectra of pure CS, HA, TCS, and HA-TCS-CS-NPs is presented in Fig. 2A. The results depict that the intense characteristic peaks of CS were appeared at 3376.74 cm^{-1} (−OH stretching), 2881.28 cm^{-1} (C−H stretching), 1659.10 cm^{-1} (C=O stretching), 1597.50 cm^{-1} (N−H bending), 1324.67 cm^{-1} and 1256.34 cm^{-1} (C−N stretching) and 1079.45 cm^{-1} (C−O−C stretching) (Hussain, Katas, Mohd Amin, Kumulosasi, Buang, et al., 2013). The standard spectra of HA depicts

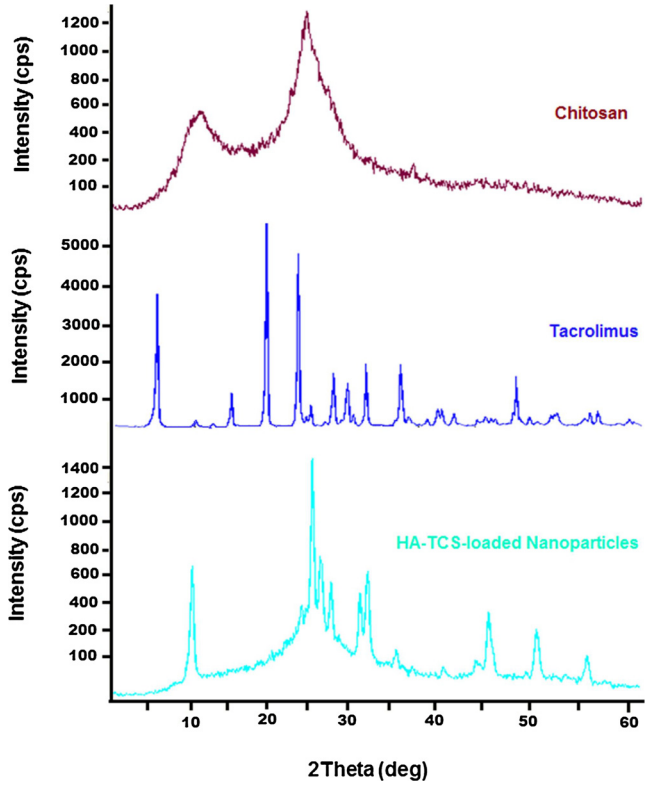

Fig. 3. XRD patterns of chitosan, tacrolimus, and HA-TCS-CS-NPs.

the characteristic peaks at 3406.48 cm^{-1} (−OH stretching), 2899.91 cm^{-1} (C−H stretching), 1617.72 cm^{-1} (N−H bending), 1410.76 cm^{-1} (combination of C−O and C═O), and 1044.11 cm^{-1} and 613.47 cm^{-1} (C−O−C stretching). The characteristics peaks of TCS appeared at 3848.12 cm^{-1} 3567.68 cm^{-1} and (−OH stretching), 3234.15 cm^{-1} and 3021.14 cm^{-1} (−CH stretching), 1833.45 cm^{-1} (C═O stretching), 1777.42 cm^{-1} (C═C stretching), and 1590.14 cm^{-1} and 1382.14 cm^{-1} (−CH stretching). For HA-TCS-CS-NPs, the characteristic peak of CS at 3376.74 cm^{-1} shifted to 3275.13 cm^{-1}. This may be due to enhanced hydrogen bonding (−OH stretching) between the CS, TCS and HA. Similarly, a shift from 2881.28 cm^{-1} to 2935.17 cm^{-1} (C−H stretching) was observed and the peak was appeared to be sharper in the HA-TCS-CS-NPs. This may also indicate that the hydrogen bonding is enhanced (Qi, Xu, Jiang, Hu, & Zou, 2004). The amide 1 bending slightly shifted from 1659.10 cm^{-1} to 1646.54 cm^{-1}; however, the amide 2 shifted from 1597.50 cm^{-1} to 1567.47 cm^{-1}. Hence there may be interaction between the $-NH_3^+$ groups of CS, TCS and HA within the HA-TCS-CS-NPs spectra (Hussain, Katas, Mohd Amin, Kumulosasi, Buang, et al., 2013). Most of the peaks obtained in HA-TCS-CS-NPs shared relatively similar position when compared to the respective standards of CS, TCS and HA. Thus, these results indicated that TCS has been successfully encapsulated into the CS-NPs and HA is coated on to the surface of HA-TCS-CS-NPs.

3.5. TGA analysis

To evaluate the thermal behaviour of HA-TCS-CS-NPs, TGA analysis was executed (Fig. 2B). Typical curve of TGA for CS showed a gradual weight loss in three stages. The weight loss in the first stage was about 7% between 50–150 °C. This could be due to dehydration of bound and adsorbed water. Second stage of weight loss started at 250 °C and continued up to 370 °C which resulted in 43% weight loss due to the degradation of CS. These findings are also in agreement with a previous study (Ziegler-Borowska, Chełminiak, Kaczmarek, & Kaczmarek-Kędziera, 2016). Towards the last stage, the thermal degradation

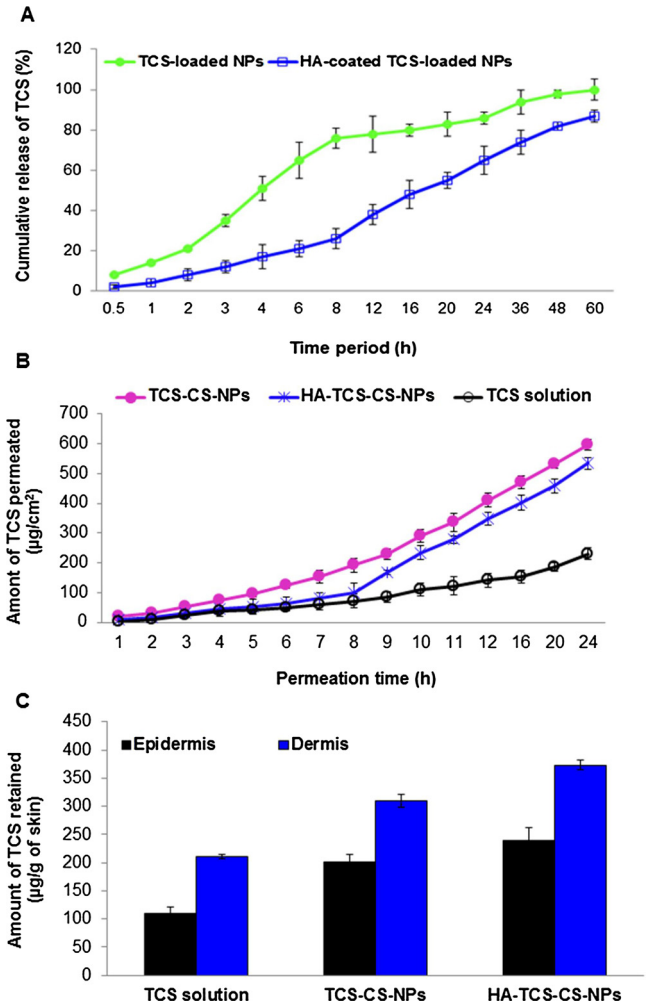

Fig. 4. (A) *In vitro* drug release of TCS from HA-TCS-CS-NPs compared to TCS-CS-NPs, (B) amount of TCS permeated from HA-TCS-CS-NPs compared to TCS-CS-NPs and TCS solution, (C) amount of TCS retained in the epidermis and the dermis from HA-TCS-CS-NPs compared to the TCS-CS-NPs and TCS solution. Data is presented as mean ± S.D (n = 3).

increased due to the decomposition of residual carbon (Ziegler-Borowska et al., 2016). Similarly, TCS exhibited three stages of weight loss. Initially, there was a slight weight loss of about 9% of drug contents between 50–220 °C followed by a steep peak of weight loss of about 42% drug contents which represents TCS degradation at 220–275 °C. The third stage of degradation started at 275 °C and 520 °C with a total weight loss of ~42% drug contents. Further analysis revealed that incorporation of TCS and HA coating on CS-NPs shifted the onset of degradation of TCS slightly earlier at 200 °C (Fig. 2B). This slow degradation continued up to 280 °C with a greater weight loss of ~50%. The second degradation phase was started at 280 °C onward and resulted in the weight loss of remaining drug contents. These changes depict a decreased thermal stability of HA-TCS-CS-NPs. The stability of this compound was determined by the intra- and inter-molecular hydrogen bonds which were influenced by water content and degree of crosslinking between the chains (Ziegler-Borowska et al., 2016).

3.6. XRD analysis

To evaluate the crystalinity and amorphous nature of CS, TCS, and HA-TCS-CS-NPs, we performed XRD analysis (Fig. 3). Broader peaks for CS were observed at 2θ, 19.7 and 20.2. These results are in line with the

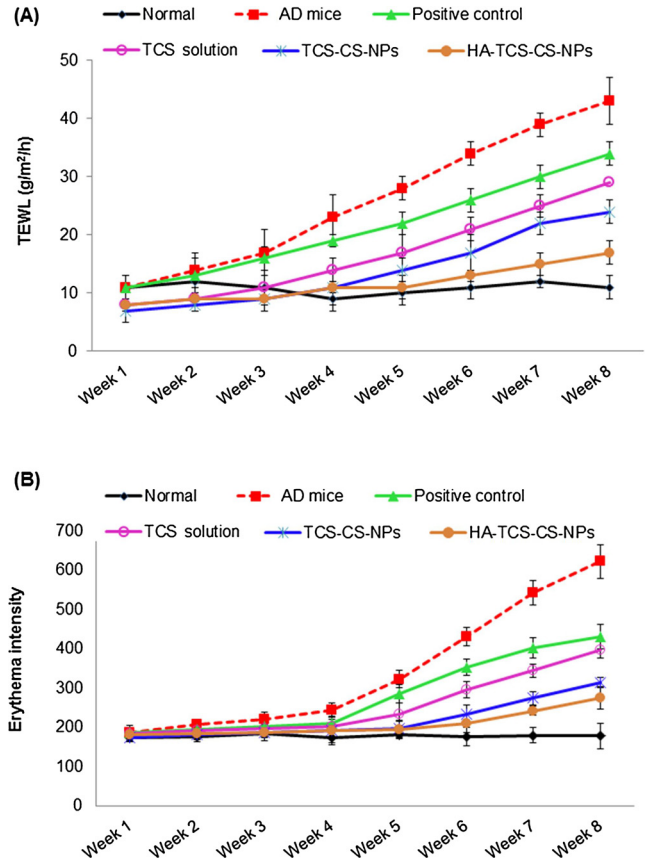

Fig. 5. Preclinical evaluation of HA-TCS-CS-NPs compared to the normal, AD mice, positive control, TCS solution, and TCS-CS-NPs groups: (A) TEWL and (B) erythema intensity. Data are presented as mean ± S.D (n = 3).

previous literature depicting amorphous nature of CS (Nunthanid, Puttipipatkhachorn, Yamamoto, & Peck, 2001). Besides that, intense peaks were observed at 2θ, 8.4, 12.5, 14.3, 14.5 in the diffraction pattern of pure TCS which indicates that TCS is a crystalline powder. HA-TCS-CS-NPs demonstrated narrower peaks at 9.5 and 17.9° compared to CS and TCS due to the encapsulation of crystalline TCS in the HA-TCS-CS-NPs. However, in comparison with the diffraction pattern of TCS, lower crystalline peaks at 20.3 and 25.3° were observed. Through the interaction between CS, TCS and HA in HA-TCS-CS-NPs, the crystallinity of TCS has been decreased and solubility has been improved.

3.7. *In vitro* drug release kinetics

To comprehend the release mechanism of TCS from HA-TCS-CS-NPs, we have performed *in vitro* release studies using dialysis tubing and the results were compared with release profile from TCS-CS-NPs (Fig. 4A). The *in vitro* drug release behaviour was investigated under the physiological conditions (pH 7.4) at 37 °C. The *in vitro* drug release results demonstrated that TCS-CS-NPs showed biphasic release pattern with rapid release rate followed by a sustained releasing phase. Results showed that ~75% of TCS released in first 8 h followed by a slow release of ~25% drug contents until 60 h (Fig. 4A). A rapid release of TCS in the first 8 h indicates the release of surface absorbed drug and the sustained release phase represents the amount of drug released from the inner core (polymeric matrices) of the NPs as a result of polymer erosion. On the other hand, HA-TCS-CS-NPs also exhibited biphasic release profiles; however, the first releasing phase demonstrated controlled and sustained release profile followed by a slightly rapid release profile. In the first 8 h, ~25% of TCS was released followed by 75% drug release until 60 h (Fig. 4A). Comparative analysis of ~25% TCS released from HA-TCS-CS-NPs system compared to ~75% release in case of TCS-CS-NPs in the first 8 h validated that HA coating provides an additional barrier for drug diffusion with regards to electrostatic interactions between the positively charged CS-NPs and negatively charged HA (Puttipipatkhachorn, Nunthanid, Yamamoto, & Peck, 2001). Moreover, HA may restrict the water diffusion into the polymeric matrix which subsequently slows down the rate of drug release (Puttipipatkhachorn et al., 2001). Hence, HA coating on to the surface of HA-TCS-CS-NPs results into a more sustained and controlled released system.

3.8. *Ex vivo* drug permeation

Despite of evaluating the *in vitro* release profile of TCS from HA-TCS-CS-NPs, the *ex vivo* permeation efficiency of TCS was also determined across the full-thickness mouse skin and the permeation data was compared with TCS-CS-NPs and the TCS solution (Fig. 4B). Results showed that the total amount of TCS permeated across the full-thickness mouse skin from TCS-CS-NPs was 3594 μg/cm^2 compared to the total amount of TCS permeated in case of HA-TCS-CS-NPs (2826 μg/cm^2) and TCS solution (1318 μg/cm^2) (Fig. 4B). These results depicted that the permeation efficiency of TCS was considerably higher in case of TCS-CS-NPs compared to HA-TCS-CS-NPs. The corresponding permeation flux (J/h) from the TCS-CS-NPs was ~194 μg/cm^2/h compared to ~118 μg/cm^2/h from HA-TCS-CS-NPs and ~55.8 μg/cm^2/h in case of TCS solution.

The comparative analysis of permeation data revealed that lowest permeation of TCS was observed in case of TCS solution which is due to the barrier properties and selective permeability of the SC. The permeation flux of TCS measured in case of HA-TCS-CS-NPs formulation was significantly ($p < 0.05$, one way ANOVA) lowered compared to TCS-CS-NPs. The lowered penetration of TCS from the HA-TCS-CS-NPs system was expected to be due to the mucoadhesive properties of HA which might have caused the HA-TCS-CS-NPs to remain adhered to the skin appendages and discharge the drug contents in a sustained manner. The mucoadhesive characteristic of the HA-TCS-CS-NPs system suggests that it would be more efficient for prolonged target specific delivery of TCS topically and may reduce frequency of topical application.

3.9. Drug retention in the epidermis and dermis

To assess the biopharmaceutical efficiency of HA-TCS-CS-NPs, we estimated the amount of TCS delivered into the various skin layers (epidermis and dermis) and the results were compared with TCS-CS-NPs and TCS solution (Fig. 4C). Results showed that highest amount of TCS retained in the epidermis (~240 ± 13.4 μg/g of skin tissue) and the dermis (~373 μg/g of skin tissue) was achieved in case of HA-TCS-CS-NPs. This amount of TCS retained in both of the skin layers was significantly ($p < 0.05$, one way ANOVA) higher compared to the TCS-CS-NPs in the epidermis (~201 ± 7.7 μg/g of skin tissue) and the dermis (~310 ± 11 μg/g of skin tissue) (Fig. 4C). The lowest amount of TCS was retained in both of the skin layers in case of TCS solution which might be associated with the lowest permeation of TCS across the SC. These findings clearly evidenced the highest potential of HA-TCS-CS-NPs to achieve significantly higher drug deposition in the epidermis and the dermis which supports our hypothesis for the target-specific (dermal) targeting of TCS for the rational management of AD. For inflammatory skin diseases like AD, it is desirable to retain drug contents in the skin layers to accomplish a site-specific therapeutic response (Hussain, Katas, Mohd Amin, Kumulosasi, Sahudin, 2013; Pople & Singh, 2012). To accomplish it, the surface of TCS-CS-NPs was modified with HA to provide distinct biopharmaceutical characteristics, occlusive effects (to enhance skin contact time), and to facilitate hydration of the SC in order to facilitate drug permeation across the SC.

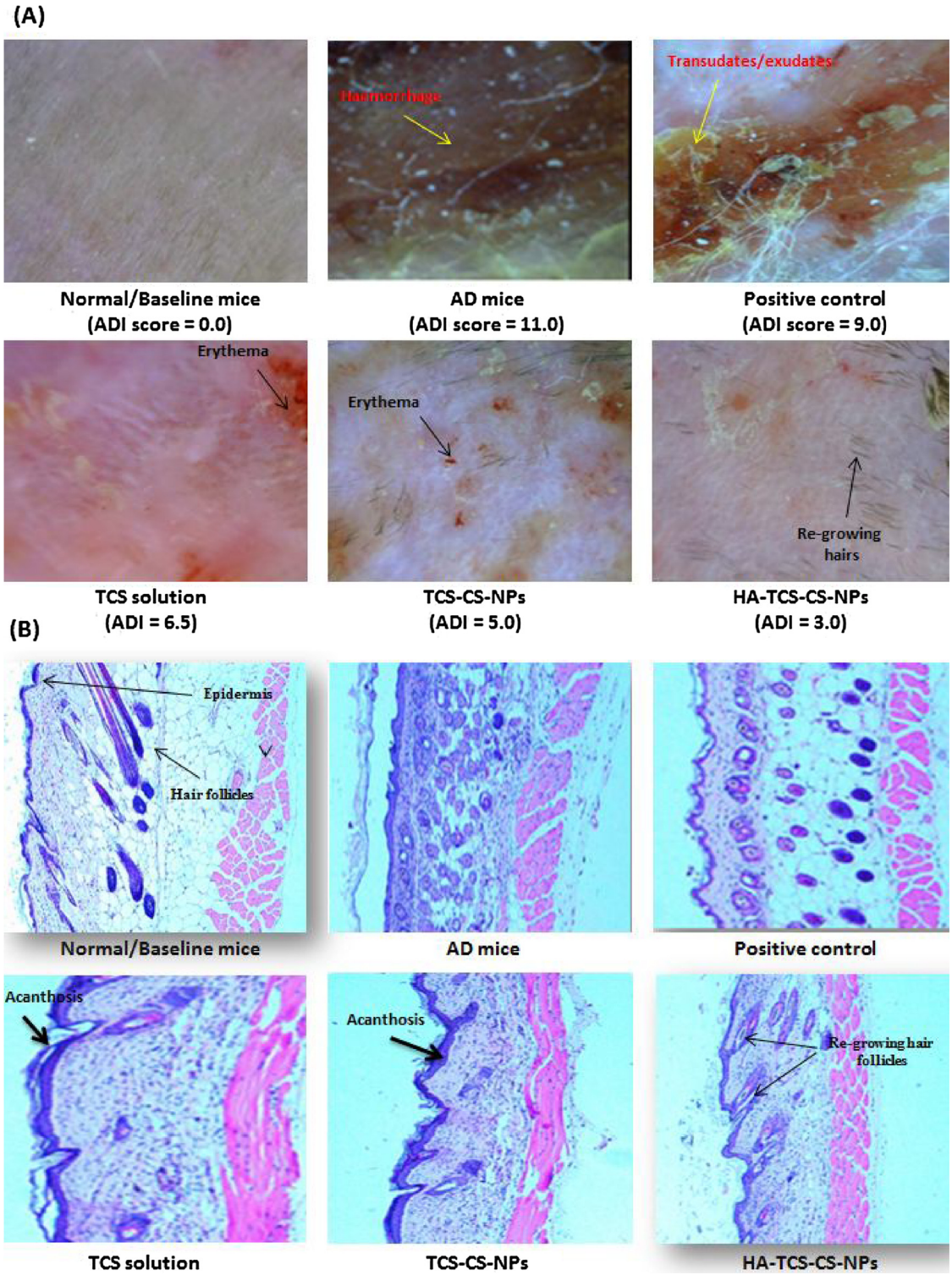

Fig. 6. (A) Dino-Lite® microscopic images of normal/baseline, AD mice, positive control, TCS solution, TCS-CS-NPs, and HA-TCS-CS-NPs treated NC/Nga mice, (B) histological examination of HA-TCS-CS-NPs treated animals compared to the normal/baseline, AD mice, TCS solution, and TCS-CS-NPs treated mice. Skin specimens were stained with H&E and imaged at ×100 μm magnification.

3.10. Evaluation of therapeutic efficacy

3.10.1. TEWL and erythema intensity

The underlying inflammatory cascades occur in AD cause severe damage to SC which led to enhance TEWL and erythema intensity. Therefore, we evaluated TEWL ($g/m^2/h$) and intensity of erythema in all experimental animals (Fig. 5A). Results showed that all test groups experienced progressive increase in the TEWL and erythema intensity from week 1 to 8; however, the animals treated with HA-TCS-CS-NPs showed minimal perturbation (Fig. 5A). This might be due to the synergistic effects of HA to promote regeneration of the SC (Davidenko, Campbell, Thian, Watson, & Cameron, 2010; Jin et al., 2012) as well as the strong anti-inflammatory efficacy and immunomodulation by TCS. A comparative TEWL analysis between the HA-TCS-CS-NPs and TCS-CS-

NPs revealed that HA exhibits additional pharmacological effects when coated on the surface of TCS-CS-NPs. On the other hand, the comparison of nanoformulations (HA-TCS-CS-NPs and TCS-CS-NPs) with TCS solution indicated that CS in the form of NPs might also facilitated reduction of TEWL by imparting positive effects on wound healing and collagen regeneration (Fig. 5A).

Despite of evaluating the TEWL, we have also assessed erythema intensity of all experimental groups (Fig. 5B). Results showed that the erythema values for all experimental groups were increased during the course of AD treatment; however, in case of nanoformulations (TCS-CS-NPs and HA-TCS-CS-NPs) very minimal erythema intensity was observed (Fig. 5B). A comparative analysis indicated that HA-TCS-CS-NPs showed superior control over the erythema intensity compared to the TCS-CS-NPs. This might be due to the accumulation of therapeutic quantities of HA and TCS in the epidermis and the dermis achieved in case of HA-TCS-CS-NPs (Hussain, Katas, Mohd Amin, Kumolosasi, & Sahudin, 2014).

3.10.2. Dermatitis severity: DinoLite® microscopic analysis

To investigate the therapeutic efficacy of HA-TCS-CS-NPs in comparison with all test groups, dermatitis score was also evaluated as the representative symptom using the DinoLite® microscope. The resulting micrograph taken from AD mice group displayed highest severity of AD (AD score = 11.0) symptoms including severe erythema, haemorrhage, oedema, superficial erosion, deep excoriation, intense itching and dryness (Fig. 6A) compared to the normal mice (AD score 0.0). The dermatitis index of the mice group treated with positive control showed less intense symptoms (AD score = 9.0) compared to the AD mice. Though, the experimental animals treated with TCS solution showed better control over AD symptoms (AD score = 6.5); however, a severe inflammation and greater erythema intensity were still obvious in these animals. The mice treated with nanoformulations (TCS-CS-NPs and HA-TCS-CS-NPs) showed greater control over the development of DNFB-induced AD-like skin lesions (Fig. 6A). More specifically, the HA-TCS-CS-NPs displayed superior efficacy ($p < 0.001$, one way ANOVA) in maintaining the skin integrity throughout the course of induction and treatment and showed only minimal symptoms of dryness and erythema. The superior anti-AD efficacy of HA-TCS-CS-NPs is expected to be due to the optimal localized targeting of TCS in the epidermis and the dermis. This localized delivery of drugs might lead to enhanced anti-inflammatory and immunomodulatory activities.

3.11. Histological examination

The therapeutic effectiveness of HA-TCS-CS-NPs formulation was also assessed by histological examination (Fig. 6B). Fig. 6B depicts that AD-induced atopic mice exhibited pronounced epidermal hyperplasia, acanthosis, hyperkeratosis, fragmented keratinised epithelium, and a large number of infiltrated inflammatory cells in the papillary dermis. These pathological features were in response to the highest grades of allergic inflammatory reaction beneath the skin due to repeated applications of DNFB. Analysis of photomicrographs obtained from AD mice further reveals that the outer keratinised epidermal layer is separated from the inner intact epidermal layer, and this might has caused by the ruthless scratching of the dorsal body region due to severe itching/rashes episodes. The photomicrographs of positive control group showed similar pathologic features to the AD mice; however, having less severe hyperkeratosis and acanthosis and less number of infiltrated cells. In contrast, AD-induced mice treated with TCS solution showed better control over infiltration of inflammatory cells and exhibited minimal epidermal hyperplasia and hyperkeratosis. Fig. 6B also depicted that AD-induced mice treated with nanoformulations (TCS-CS-NPs and HA-TCS-CS-NPs) showed minimal infiltration of inflammatory cells in the dermis and lowest degree of acanthosis. In particular, the mice treated with HA-TCS-CS-NPs also exhibited inter-digitations between the epidermis and dermis with greater developed hair follicles as was observed in the normal mice. This finding indicates the restoration of the skin integrity in the NC/Nga mice treated with HA-TCS-CS-NPs formulation.

4. Conclusion

Nano-delivery systems (including the polymeric nanoparticles) have gained remarkable recognition from scientists/researchers due to their nano-range sizes, surface charges, high entrapment efficiency, targeted delivery of drugs, avoidance of premature degradation of labile compounds, and improved pharmacokinetic profile and therapeutic efficacy of pharmacological moieties. Therefore, we aimed to fabricate CS-NPs for targeted delivery of TCS to deeper layers of the skin. To further improve their targeting efficiency and additional pharmacological advantages, we decorated the TCS-CS-NPs with HA. Following a series of optimization experiments, the HA-TCS-CS-NPs with optimum physicochemical characteristics (particle size, zeta potential, PDI, %EE, and % LC) were successfully prepared using high pressure homogenisation–solvent evaporation method. The characteristic difference between the FTIR spectra, XRD diffractograms, and TGA spectra evidenced the successful loading of TCS and coating with HA, improved thermal stability and crystallinity. The results of *in vitro* drug release revealed that HA-TCS-CS-NPs follow a sustained release pattern compared to the TCS-CS-NPs. Taken together, the HA-TCS-CS-NPs showed efficient dermal targeting by significantly enhanced percentage of TCS retained in the epidermis and the dermis and improved therapeutic efficacy. The pre-clinical evaluations of our nanoformulation (HA-TCS-CS-NPs) displayed pronounced anti-AD efficacy by progressive reduction in the rate of TEWL, erythema intensity, and dermatitis index. With these findings, we anticipate that this innovative nanocarrier-based formulation (HA-TCS-CS-NPs) could be a promising tool for percutaneous delivery of anti-inflammatory and immunomodulatroy agents for treatment of AD. Nevertheless, further studies including systemic toxicity, pharmacokinetic profile of TCS, and mechanism of anti-AD efficacy are recommended to authenticate the safety and pharmacodynamics profile of this nanodelivery system.

Declaration of interest

The authors report no declaration of interest in the present work.

Acknowledgements

The authors would like to acknowledge Institute of Research Management & Innovation (IRMI), Universiti Teknologi MARA (UiTM) for providing LESTARI grants (600-IRMI/DANA 5/3/LESTARI (0007/2016)).

References

Amidi, M., Romeijn, S. G., Borchard, G., Junginger, H. E., Hennink, W. E., & Jiskoot, W. (2006). Preparation and characterization of protein-loaded N-trimethyl chitosan nanoparticles as nasal delivery system. *Journal of Controlled Release, 111*(1–2), 107–116.

Benoit, D. N., Zhu, H., Lilierose, M. H., Verm, R. A., Ali, N., Morrison, A. N., et al. (2012). Measuring the grafting density of nanoparticles in solution by analytical ultracentrifugation and total organic carbon analysis. *Analytical Chemistry, 84*(21), 9238–9245.

Bhattacharjee, S. (2016). DLS and zeta potential - What they are and what they are not? *Journal of Controlled Release, 235*, 337–351.

Bieber, T. (2008). Atopic dermatitis. *The New England Journal of Medicine, 358*(14), 1483–1494.

Davidenko, N., Campbell, J. J., Thian, E. S., Watson, C. J., & Cameron, R. E. (2010). Collagen–hyaluronic acid scaffolds for adipose tissue engineering. *Acta Biomaterialia, 6*(10), 3957–3968.

Hussain, Z., Sahudin, S., Thu, H. E., Shuid, A. N., Bukhari, S. N., & Kumolosasi, E. (2016). Recent advances in pharmacotherapeutic paradigm of mild to recalcitrant atopic dermatitis. *Critical Reviews in Therapeutic Drug Carrier Systems, 33*(3), 213–263.

Hussain, Z., Thu, H. E., Katas, H., & Bukhari, S. N. A. (2017). Hyaluronic acid-based biomaterials: A versatile and smart approach to tissue regeneration and treating

traumatic, surgical, and chronic wounds. *Polymer Reviews, 57*, 594–630.
Hussain, Z., Katas, H., Mohd Amin, M. C. I., & Kumolosasi, E. (2014). Efficient immunomodulation of TH1/TH2 biomarkers in 2,4-dinitrofluorobenzene-induced atopic dermatitis: Nanocarrier-mediated transcutaneous co-delivery of anti-inflammatory and antioxidant drugs. *PLoS One, 9*(11), e113143.
Hussain, Z., Katas, H., Mohd Amin, M. C. I., Kumolosasi, E., Buang, F., & Sahudin, S. (2013). Self-assembled polymeric nanoparticles for percutaneous co-delivery of hydrocortisone/hydroxytyrosol: An ex vivo and in vivo study using an NC/Nga mouse model. *International Journal of Pharmaceutics, 444*, 109–119.
Hussain, Z., Katas, H., Mohd Amin, M. C. I., Kumolosasi, E., & Sahudin, S. (2014). Downregulation of immunological mediators in 2,4-dinitrofluorobenzene-induced atopic dermatitis-like skin lesions by hydrocortisone-loaded chitosan nanoparticles. *International Journal of Nanomedicine, 9*, 5143–5156.
Hussain, Z., Katas, H., Mohd Amin, M. C. I., Kumulosasi, E., & Sahudin, S. (2013). Antidermatitic perspective of hydrocortisone as chitosan nanocarriers: An ex vivo and in vivo assessment using an NC/Nga mouse model. *Journal of Pharmaceutical Sciences, 102*, 1063–1075.
Jin, Y. J., Termsarasab, U., Ko, S. H., Shim, J. S., Chong, S., Chung, S. J., et al. (2012). Hyaluronic acid derivative-based self-assembled nanoparticles for the treatment of melanoma. *Pharmaceutical Research, 29*(12), 3443–3454.
Kalam, M. A. (2016). Development of chitosan nanoparticles coated with hyaluronic acid for topical ocular delivery of dexamethasone. *International Journal of Biological Macromolecules, 89*, 127–136.
Katas, H., & Alpar, H. O. (2006). Development and characterisation of chitosan nanoparticles for siRNA delivery. *Journal of Controlled Release, 115*(2), 216–225.
Mainardes, R. M., & Evangelista, R. C. (2005). PLGA nanoparticles containing praziquantel: Effect of formulation variables on size distribution. *International Journal of Pharmaceutics, 290*(1–2), 137–144.
Maiolino, S., Russo, A., Pagliara, V., Conte, C., Ungaro, F., Russo, G., et al. (2015). Biodegradable nanoparticles sequentially decorated with polyethyleneimine and hyaluronan for the targeted delivery of docetaxel to airway cancer cells. *Journal of Nanobiotechnology, 13*, 29.
Nunthanid, J., Puttipipatkhachorn, S., Yamamoto, K., & Peck, G. E. (2001). Physical properties and molecular behavior of chitosan films. *Drug Development and Industrial Pharmacy, 27*(2), 143–157.
Padula, C., Sartori, F., Marra, F., & Santi, P. (2005). The influence of iontophoresis on acyclovir transport and accumulation in rabbit ear skin. *Pharmaceutical Research, 22*, 1519–1524.
Pandey, M., Choudhury, H., Gunasegaran, T. A. P., Nathan, S. S., Md, S., Gorain, B., et al. (2018). Hyaluronic acid-modified betamethasone encapsulated polymeric nanoparticles: Fabrication, characterisation, in vitro release kinetics, and dermal targeting. *Drug Delivery and Translational Research*(February), http://dx.doi.org/10.1007/s13346-018-0480-1.
Parida, U. K., Rout, N., & Bindhani, B. K. (2013). In vitro properties of chitosan nanoparticles induce apoptosis in human lymphoma SUDHL-4 cell line. *Advances in Bioscienc and Biotechnology, 4*, 1118–1127.
Park, E., Park, K., Eo, H., Seo, J., Son, M., Kim, K., et al. (2007). Suppression of spontaneous dermatitis in NC/Nga murine model by PG102 isolated from Actinidia arguta. *Journal of Investigative Dermatology, 127*, 1154–1160.
Peng, J., Dong, W. J., Li, L., Xu, J. M., Jin, D. J., Xia, X. J., et al. (2015). Effect of high-pressure homogenization preparation on mean globule size and large-diameter tail of oil-in-water injectable emulsions. *Journal of Food and Drug Analysis, 23*(4), 828–835.
Pople, P. V., & Singh, K. K. (2012). Targeting tacrolimus to deeper layers of skin with improved safety for treatment of atopic dermatitis-part II: In vivo assessment of dermatopharmacokinetics, biodistribution and efficacy. *International Journal of Pharmaceutics, 434*(1–2), 70–79.
Puttipipatkhachorn, S., Nunthanid, J., Yamamoto, K., & Peck, G. E. (2001). Drug physical state and drug-polymer interaction on drug release from chitosan matrix films. *Journal of Controlled Release, 75*(1–2), 143–153.
Qi, L., Xu, Z., Jiang, X., Hu, C., & Zou, X. (2004). Preparation and antibacterial activity of chitosan nanoparticles. *Carbohydrate Research, 339*, 2693–2700.
Safdar, M. H., Hussain, Z., Abourehab, M. A. S., Hasan, H., Afzal, S., & Thu, H. E. (2017). New developments and clinical transition of hyaluronic acid-based nanotherapeutics for treatment of cancer: Reversing multidrug resistance, tumour-specific targetability and improved anticancer efficacy. *Artificial Cells, Nanomedicine and Biotechnology*, 1–14. http://dx.doi.org/10.1080/21691401.2017.1397001.
Shao, M., Hussain, Z., Thu, H. E., Khan, S., Katas, H., Ahmed, T. A., et al. (2016). Drug nanocarrier, the future of atopic diseases: Advanced drug delivery systems and smart management of disease. *Colloids and Surfaced B: Biointerfaces, 147*, 475–491.
Sharma, N., Madan, P., & Lin, S. (2016). Effect of process and formulation variables on the preparation of parenteral paclitaxel-loaded biodegradable polymeric nanoparticles: A co-surfactant study. *Asian Journal of Pharmaceutical Sciences, 11*, 404–416.
Tay, Y. K., Kong, K. H., Khoo, L., Goh, C. L., & Giam, Y. C. (2002). The prevalence and descriptive epidemiology of atopic dermatitis in Singapore school children. *British Journal of Dermatology, 146*(1), 101–106.
Wang, T., Hou, J., Su, C., Zhao, L., & Shi, Y. (2017). Hyaluronic acid-coated chitosan nanoparticles induce ROS-mediated tumor cell apoptosis and enhance antitumor efficiency by targeted drug delivery via CD44. *Journal of Nanobiotechnology, 15*, 7.
Witting, M., Boreham, A., Brodwolf, R., Vávrová, K., Alexiev, U., Friess, W., et al. (2015). Interactions of hyaluronic acid with the skin and implications for the dermal delivery of biomacromolecules. *Molecular Pharmaceutics, 12*(5), 1391–1401.
Wu, X., Price, G. J., & Guy, R. H. (2009). Disposition of nanoparticles and an associated lipophilic permeant following topical application to the skin. *Molecular Pharmaceutics, 6*(5), 1441–1448.
Yin, Z., Xu, J., & Luo, D. (2011). Efficacy and tolerance of tacrolimus and pimecrolimus for atopic dermatitis: A meta-analysis. *Journal of Biomedical Research, 25*(6), 385–391.
Ziegler-Borowska, M., Chełminiak, D., Kaczmarek, H., & Kaczmarek-Kędziera, A. (2016). Effect of side substituents on thermal stability of the modified chitosan and its nanocomposites with magnetite. *Journal of Thermal Analysis and Calorimetry, 124*(3), 1267–1280.
Zöller, N. N., Kippenberger, S., Thaçi, D., Mewes, K., Spiegel, M., Sättler, A., et al. (2008). Evaluation of beneficial and adverse effects of glucocorticoids on a newly developed full-thickness skin model. *Toxicology In Vitro, 22*(3), 747–759.
Zu, Y., Zhang, Y., Wang, W., Zhao, X., Han, X., Wang, K., et al. (2014). Preparation and *in vitro/in vivo* evaluation of resveratrol-loaded carboxymethyl chitosan nanoparticles. *Drug Delivery, 23*(3), 981–991.